Heliyon 9 (2023) e17844

Contents lists available at ScienceDirect

Heliyon

journal homepage: www.cell.com/heliyon

The role of microbial metabolites in diabetic kidney disease

Ting Zhu [a,1], Bi-Ying Hu [b,1], Yi-Qing Zhang [a,1], Ze-Yu Zhang [b], Kai-Wen Cai [a], Lei Lei [a], Bo Hu [b], Xiao-Hua Wang [a], Chun Tang [a,***], Yong-Ping Lu [a,b,*], Zhi-Hua Zheng [a,**]

[a] Department of Nephrology, Center of Kidney and Urology, the Seventh Affiliated Hospital, Sun Yat-sen University, Shenzhen, China
[b] Department of Nephrology, the First Affiliated Hospital of Jinan University, Guangzhou, China

ARTICLE INFO

Keywords:
Diabetic kidney disease
Gut microbial metabolism
Glycerophospholipid metabolism
Tryptophan metabolism

ABSTRACT

Background: Growing evidence suggests a complex bidirectional interaction between gut microbes, gut-derived microbial metabolites, and diabetic kidney disease (DKD), known as the "gut-kidney axis" theory. The present study aimed to characterize the role of microbial metabolites in DKD.

Methods: Six-week-old db/db and littermate db/m mice were raised to 20 weeks old. The serum, urine, feces, liver, perinephric fat, and kidney were analyzed using liquid chromatography with tandem mass spectrometry (LC-MS/MS)-based metabolomic analyses.

Results: The db/db mice showed obvious pathological changes and worse renal functions than db/m mice. Indoleacetaldehyde (IAld) and 5-hydroxy-L-tryptophan (5-HTP) in kidney samples, and serotonin (5-HT) in fecal samples were increased in the db/db group. Phosphatidylcholine (PC), phosphatidate (PA), and 1-acylglycerophosphocholine (lysoPC) were decreased in liver and serum samples of the db/db group, while PC and lysoPC were decreased in kidney and perinephric fat samples. Suggested metabolomic homeostasis was disrupted in DKD mice, especially glycerophospholipid and tryptophan metabolism, which are closely related to the gut microbiome.

Conclusions: Our findings reveal the perturbation of gut microbial metabolism in db/db mice with DKD, which may be useful for building a bridge between the gut microbiota and the progression of DKD and provide a theoretical basis for the intestinal treatment of DKD.

1. Introduction

Diabetes mellitus (DM) affects approximately 10% of the global population [1], and its morbidity and mortality are mainly related to complications of multiple organ systems, such as the kidneys. Moreover, approximately 40% of the diabetes cases progress to diabetic nephropathy (DKD), which is the prime reason of chronic kidney disease (CKD) globally and leads to kidney failure [2]. Despite the tight control of blood sugar and lipids in patients with DKD, renal function often remains poor, partly due to the limited

* Corresponding author. Department of Nephrology, Center of Kidney and Urology, the seventh affiliated Hospital, Sun Yat-sen University, Shenzhen, China.
** Corresponding author.
*** Corresponding author.
E-mail addresses: tangchun@sysush.com (C. Tang), luyongping@sysush.com (Y.-P. Lu), zhzhihua@mail.sysu.edu.cn (Z.-H. Zheng).
[1] Ting Zhu, Bi-Ying Hu and Yi-Qing Zhang contributed equally to this work and share first authorship.

https://doi.org/10.1016/j.heliyon.2023.e17844
Received 14 November 2022; Received in revised form 21 June 2023; Accepted 29 June 2023
Available online 4 July 2023

cognition of the complex metabolic processes of DKD [3,4].

DKD is related to many metabolic pathways and complex metabolic pathology [5,6]. Intestinal bacteria produced by the host organism produce metabolites, such as short-chain fatty acids [7]and uremic toxins [8]. These metabolites act as a bridge between DKD and gut microbiota, and can more directly reveal the mutual effect between disease and gut microbiota. The gut microbiota is considered as a key regulator of DKD development in patients with DM [9,10]. Intestinal dysbiosis leads to intestinal mucosal barrier impairment and entry of gut microbial uremic toxins into the circulatory system, which leads to systemic microinflammation, insulin resistance, and kidney damage [11]. Gut microbiota and microbial metabolites, such as tryptophan and polyamine metabolism, can mediate renal fibrosis in CKD rats [12,13]. Increasing evidence indicates a complex correlation among intestinal microbiota, gut-derived microbial metabolites, and DKD [14–16]. However, there are few studies on the effects of specific metabolites from gut microbes and exogenous substances on DKD [17]. The pathophysiological correlation between gut-derived microbial metabolites and DKD is unclear.

Metabolites are the intermediate or final products of biochemical reactions, respectively, which can match the disease phenotype and reflect the biological information of genetics, drugs, food, environment, gut microbes, and host [18]. Identifying the microbial metabolites derived from the gut of DKD and exploring their effects on multi-organ metabolism will help to unearth the precise pathogenesis of DKD and provide a theoretical basis for the intestinal treatment of DKD. In this study, we explore the possible mechanisms between the gut-serum-liver-perinephric fat-kidney metabolic axis and microbial metabolites in mice with DKD.

2. Materials & methods

2.1. Animals and research design

Male 6-week-old C57BLKS/J-leprdb/leprdb mice (db/db mice, n = 15) and matched littermate C57BLKS/J-leprdb/leprm mice (db/m mice, n = 15, as normal controls) were purchased from the Nanjing University Experimental Animal Center. All mice were fed with 10 mL/kg sterile water for 12 weeks after adaptive feeding. All mice were maintained in SPF environment (22 ± 2 °C, 55 ± 10% humidity, with a 12-h light/dark cycle) and received food/water without restriction. From the 3rd to 14th week, we recorded body weights weekly, and fasting blood glucose (FBG) every four weeks. The 24-h urine samples, whole blood samples, feces, kidney tissues, perinephric fat, and liver tissues were obtained from each mouse at the completion of the animal experiment. The whole blood samples were allowed to stand for about 1 h at room temperature and centrifuged at 3000 rpm for 10 min. After centrifugation of the whole blood samples, the upper serum was collected. All left kidneys were taken for pathological section, and the right ones were taken for metabolomics analysis. Serum and other specimens were stored at −80 °C for biochemical assays and untargeted metabolomic sequencing. The experiments in this study were carried out in line with the requirements of the Laboratory Animal Experimentation law, and were allowed by the Experimental Animal Ethics of Jinan University (approval No. 202069-04). A detailed flowchart of experiments is shown in Fig. 1a.

2.2. Biochemical analysis and histopathological examination

FBG levels were measured by a portable blood glucose meter (BAYER, Germany) and blood glucose test strips (BAYER, Germany). The levels of serum cystosin C (Cys-C) were detected using a mouse Cys-C ELISA Kit (E-EL-M3024, Elabscience, Wuhan, China). Urine creatinine (Ucr) and urine microalbumin were measured using Ucr enzyme-linked immunosorbent (ELISA) kit (MM-44289M1, Elabscience, Wuhan, China) and MAU/ALB ELISA kit (MM-0705M1, Elabscience, Wuhan, China), respectively. Blood urea nitrogen (BUN) levels were quantified using an automated biochemical analyzer (Hitachi High-Tecgnoologies, Japan). Student's t-test was used for comparison between the two groups. The formalin-fixed tissue was embedded in paraffin and cut into 4 μm thick sections, and further used for hematoxylin-eosin (H&E), Masson, and Periodic Acid Schiff (PAS) staining. The average glomerular perimeter, glomerular area, and the percentage of the fibrotic area were detected using the ImageJ software. Histological analysis was operated by two independent investigators using a blinded method.

2.3. Metabolomic analysis

2.3.1. Sample preparation

50 mg of each tissue was added in 1000 μL of internal standard mixture (methanol:acetonitrile:water in a 2:2:1 ratio). Next, the tissues were ground for 4 min at 35 Hz, and then sonicated thrice on ice bath for 5 min each. Each serum sample (50 μL) was added to internal standard mixture (acetonitrile:methanol in a 1:1 ratio, 200 μL). The serum was vortexed for 30 s and then sonicated on an ice bath for 10 min. After standing at −40 °C for 1 h, all tissues and serum samples were cryogenically centrifuged for 15 min at 4 °C and 12000r. The supernatants were collected for further testing.

2.4. LC-MS/MS analysis

The UHPLC system (Vanquish, Thermo Fisher Scientific) with UPLC BEH Amide (2.1 mm × 100 mm, 1.7 μm) combined with a Q-Exactive HFX mass spectrometer (Orbitrap MS, Thermo) was used for LC-MS/MS analysis. Mobile phase A was composed of 25 mmol/L ammonium acetate and 25 ammonia hydroxide in water, while mobile phase B was composed of acetonitrile. The detailed parameters of MS conditions can be retrieved from our published article [19].

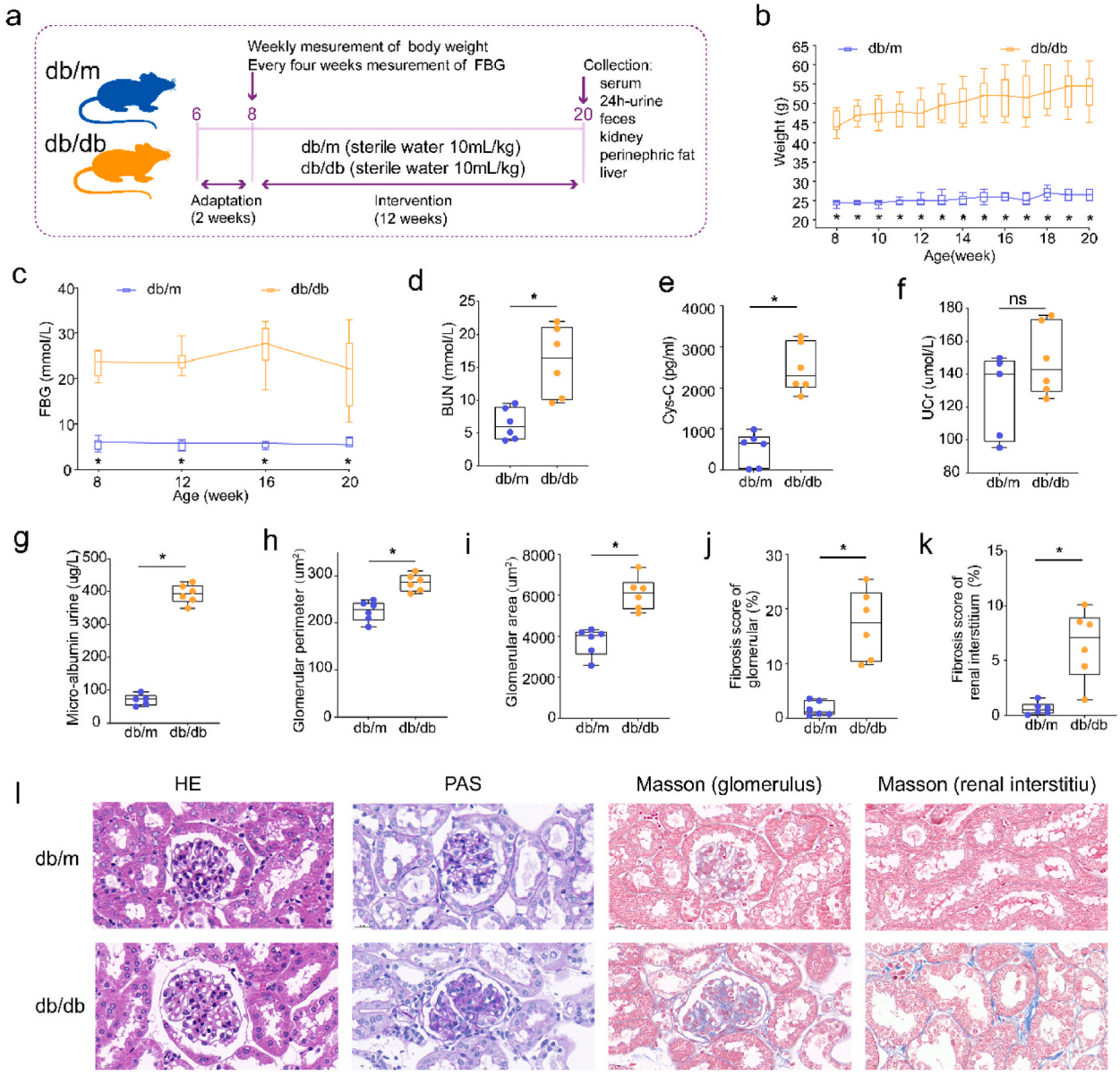

Fig. 1. Basic characteristics of db/m (n = 6) and db/db (n = 6) mice. (a) The workflow of the animal experiment. **(b)** Weight changes in mice during the intervention. **(C)** FBG levels of mice during the intervention. **(d–g)** The level of **(d)** BUN, **(e)** serum Cys-C, **(f)** UCr, and **(g)** urine microalbumin in the two groups. **(h)** The average glomerular perimeters and **(i)** glomerular area detected by H&E staining in the two groups. **(j)** The percentage of glomerular and **(k)** interstitial fibrosis detected by Masson staining in the two groups. **(l)** Representative renal tissue pathology (200×) of mice in each group (H&E staining, PAS staining, and Masson staining). *$P < 0.05$ (db/m vs. db/db); "ns", not significant. Fasting-blood glucose, FBG; blood urea nitrogen, BUN; serum cystatin C, Cys-C; urine creatinine, UCr.

2.5. Data processing

The MS data was changed into the mzXML format through the ProteoWizard software. Further raw data processing, such as peak detection, extraction, alignment, and integration, was performed using an in-house R package. The metabolites were annotated by the online database, namely Human Metabolome Database (HMDB) and Kyoto Encyclopedia of Genes and Genomes (KEGG), and a secondary MS database (BiotreeDB V2.1) with 0.3 as the cut-off. The quality control results show that the sample quality, experimental method, and system stability were reliable and suitable for subsequent metabolomic analysis. For details, see Supplementary Materials and Methods and Figs. S1–S5. The relative intensity of each metabolite was normalized using the total ion current (TIC) of each metabolite. Metabolites with >50% missing values were removed from the data, and half the minimum value superseded the remaining null values.

2.6. Statistical analysis

MetaboAnalyst 5.0 (www.metaboanalyst.ca) was used for metabolomic data analysis. Global metabolic changes between the two groups were determined using the Orthogonal partial least squares discriminate analysis (OPLS-DA) model. The model parameters R2 and Q2 served as indicators for evaluating the interpretability and predictability of the model, respectively. R2 and Q2 > 0.05 indicate that the model was robust and reliable. The OPLS-DA model produced variable importance in projection (VIP) values. Metabolites satisfying conditions ($P < 0.05$, VIP >1, and |fold change| > 1.5) were selected as differentially expressed metabolites (DEMs). The metabolic pathway enrichment analysis was performed using the pathway analysis module of Metaboanalyst 5.0. Pathways with $p < 0.05$ and impact >0.1 were considered statistically significant. The identified metabolites were classified according to the HMDB database. The DEMs were classified using MetOrigin (http://metorigin.met-bioinformatics.cn/) [20]. The DEMs from microbiota and co-metabolites were considered as gut-derived microbial metabolites. And we performed a correlation analysis of microbial metabolites and co-metabolites from feces and the serum, liver, kidney, and perinephric fat (Tables S17–S20). The levels of fecal microbial metabolites and co-metabolites were associated with the levels of microbial metabolites and co-metabolites from the serum, liver, kidney, and perinephric fat. In a correlation analysis network diagram, the variations of some microbial metabolites in feces are correlated with their variations in serum and peripheral organs (Fig. S6). Volcano plots and heat maps were generated using the R packages 'ggplot' and 'pheatmap', respectively. Spearrelations between gut-derived microbial DEMs were performed in R using the Hmisc package. Data with a correlation coefficient >0.6 were visualized as chord diagrams in R using circlize packages.

3. Results

3.1. The baseline data of db/db mice

Baseline characteristics have been described in our previously published paper [21]. The body weight, FBG, renal function index (blood urea nitrogen, Cystatin-C, urine microalbumin) were higher in db/db than db/m mice from 8th - 20th week of feeding ($P < 0.05$). The db/db mice exhibited more severe renal pathology than the db/m mice. These results suggest the development of DKD in db/db mice. The baseline data were shown in Fig. 1b–l and Table S1.

3.2. Fecal metabolite profiling in db/db mice

In all, 1255 metabolites (positive mode: 983 and negative mode: 272) were identified from fecal samples. OPLS-DA models indicate noticeable metabolic differences between the db/db and db/m feces samples (R2 = 0.995, Q2 = 0.759) (Fig. 2a). We identified that 133 metabolites were upregulated, while 20 were downregulated (Fig. 2b, Table S2). Moreover, 153 DEMs in the feces were significantly enriched in six pathways, involving three metabolic abnormalities: energy metabolism (lipid and amino acid metabolism), and cofactor and vitamin metabolism (Fig. 2c, Table S3). Based on the origin of metabolites, the DEMs were further classified into five groups as follows: host (3), microbiota (13), co-metabolite (18), exogenous (93), and unknown (26) (Fig. 2d, Table S2). Co-metabolites refer to the DEMs derived from the microbiota and host. To better understand the underlying role of the gut microbiome, we analyzed the correlations and biological functions of 31 DEMs from microbiota and co-metabolites. In metabolite-metabolite correlations, most gut-derived microbial DEMs in the network were lipids (Fig. 2e, Table S4). The pathway analysis revealed that amino acid metabolism, including tryptophan metabolism, tyrosine metabolism, and phenylalanine metabolism and glycerophospholipid metabolism were the main pathways in the db/db group (Fig. 2f, Table S3). The expression and classification of these 31 microbe-derived metabolites are shown in Fig. 2g (Table S2), and we found that lipid metabolites accounted for the most. These findings suggest that amino acid and lipid metabolism disturbances characterize gut-derived microbial metabolites in fecal metabolic profiles.

3.3. Serum metabolite profiling in db/db mice

Untargeted metabolic analysis of serum samples detected 678 metabolites (positive mode: 459 and negative mode: 219). OPLS-DA analysis of serum metabolite profiles showed differences between the db/db and db/m samples (Q2 = 0.887, R2 = 0.999) (Fig. 3a). We screened 216 serum DEMs according to the criteria mentioned in the methods, with 109 upregulated metabolites and 107 downregulated metabolites (Fig. 3b, Table S5). These DEMs were enriched in 15 pathways involving lipid metabolism, amino acid metabolism, and nucleotide metabolism (Fig. 3c, Table S6). Among 216 serum DEMs, 38 DEMs were derived from microbiota, and 67 DEMs were derived from co-metabolites (Fig. 3d, Table S5). Among 105 gut-derived microbial metabolites, we found that lipid and organic acid metabolites (mostly amino acid metabolites) had the greatest correlation with other metabolites (Fig. 3e, Table S7). Moreover, these microbe-derived metabolites were mostly enriched in glycerophospholipid metabolism, arginine and proline metabolism, and arginine biosynthesis (Fig. 3f, Table S6). The expression and classification of these 105 microbe-derived metabolites are shown in Fig. 3g (Table S5), and we found that lipid and organic acid metabolites accounted for the most.

3.4. Liver metabolite profiling in db/db mice

Untargeted metabolic analysis of liver samples detected 743 metabolites (positive mode: 526 and negative mode: 217). OPLS-DA analysis of liver metabolite profiles showed differences between the db/db and db/m samples (Q2 = 0.9, R2 = 0.995) (Fig. 4a). We screened 231 liver DEMs, with 19 upregulated and 212 downregulated metabolites (Fig. 4b, Table S8). These DEMs were mostly

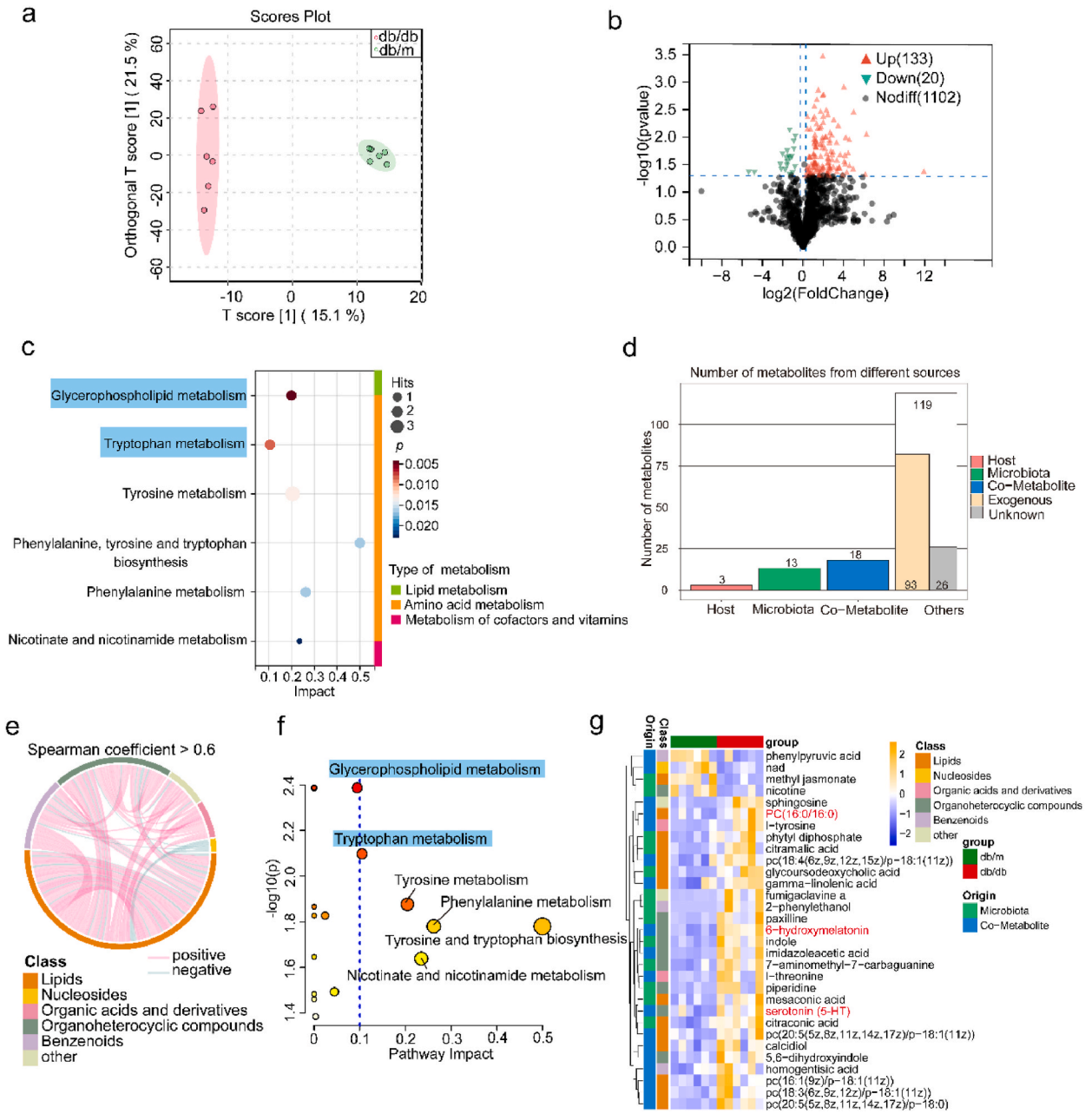

Fig. 2. Fecal metabolic profiling in db/db mice. (a) OPLS-DA score showing the conspicuous differential metabolic features of feces between db/m and db/db groups. **(b)** Volcano plot showing 153 DEMs in feces between the db/m and db/db groups. **(c)** KEGG pathway analysis of 153 DEMs in feces between the db/m and db/db groups. **(d)** Column graph showing the number of fecal DEMs from different sources. Co-metabolites refer to the DEMs derived from microbiota and host. **(e)** The chord diagram showing significant correlations between fecal DEMs of different classes or within the same class. Metabolite class is shown as a color bar around the circumference. Each line indicates a significant correlation (Spearman's correlation, $r > 0.6$, $p < 0.05$). Pink, positive correlation; Cyan, negative correlation. **(f)** KEGG pathway analysis of DEMs derived from microbiota and co-metabolites. **(g)** Heatmap of 31 DEMs derived from microbiota and co-metabolites of fecal samples. Metabolite classes and origins are shown on the left of the heatmap. The red font represents DEMs in the tryptophan metabolism and the glycerophospholipid metabolism pathway. Phosphatidylcholine, PC. (For interpretation of the references to color in this figure legend, the reader is referred to the Web version of this article.)

enriched in lipid metabolism, amino acid metabolism, and carbohydrate metabolism (Fig. 4c, Table S9). Among 231 liver DEMs, 16 DEMs were derived from microbiota, and 70 DEMs were derived from co-metabolites (Fig. 4d, Table S8). Among 86 gut-derived microbial metabolites, we found that organic acid metabolites (mostly amino acid metabolites) and lipid metabolites had the greatest correlation with other metabolites (Fig. 4e, Table S10). Moreover, these microbial metabolites were mostly enriched in glycerophospholipid metabolism, sphingolipid metabolism, ascorbate metabolism, and aldarate metabolism (Fig. 4f, Table S9). The

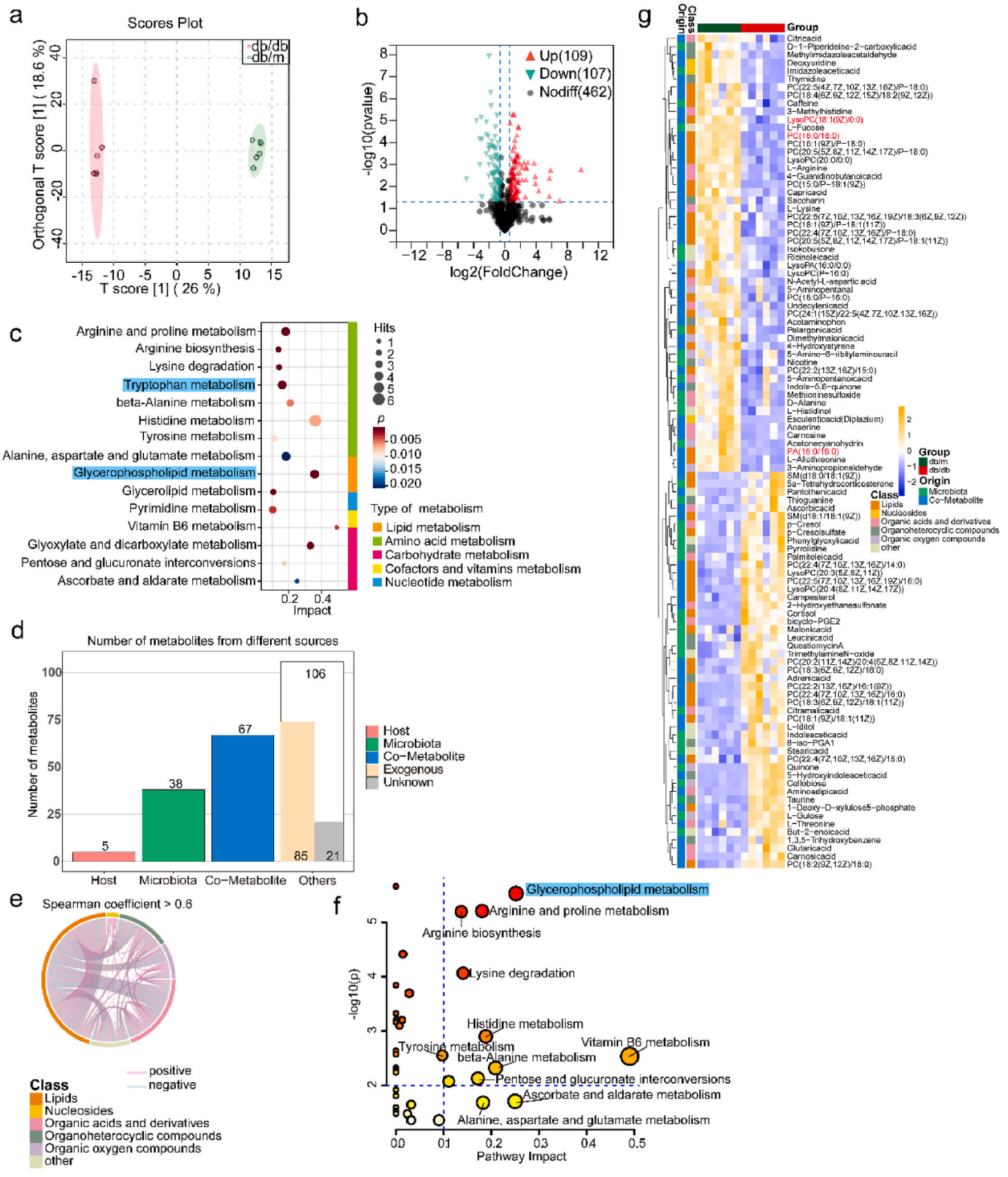

(caption on next page)

Fig. 3. Serum metabolic profiling in db/db mice. (a) OPLS-DA score showing the conspicuous differential metabolic features of serum between the db/m and db/db groups. **(b)** Volcano plot showing 216 DEMs in serum between the db/m and db/db groups. **(c)** KEGG pathway analysis of 216 serum DEMs between the db/m and db/db groups. **(d)** Column graph showing the number of serum DEMs from different sources. Co-metabolites refer to the DEMs derived from microbiota and host. **(e)** The chord diagram showing significant correlations between serum DEMs of different classes or within the same class. Metabolite class is shown as a color bar around the circumference. Each line indicates a significant correlation (Spearman's correlation, $r > 0.6$, $p < 0.05$). Pink, positive correlation; Cyan, negative correlation. **(f)** KEGG pathway analysis of DEMs derived from microbiota and co-metabolites. **(g)** Heatmap of 105 DEMs derived from microbiota and co-metabolites of serum samples. Metabolite classes and origins are shown on the left of the heatmap. The red font represents DEMs in the glycerophospholipid metabolism pathway. Phosphatidate, PA; Phosphatidylcholine, PC; 1-Acylglycerophosphocholine, lysoPC. (For interpretation of the references to color in this figure legend, the reader is referred to the Web version of this article.)

expression and classification of these 86 microbial metabolites are shown in Fig. 4g (Table S8), and we found that lipid and organic acid metabolites accounted for the most.

3.5. Perinephric fat metabolite profiling in db/db mice

500 metabolites (positive mode: 344 and negative mode: 156) were detected from perinephric fat samples. OPLS-DA models showed noticeable differences in perinephric fat metabolic profiles between the db/db and db/m samples ($Q2 = 0.851$, $R2 = 0.999$) (Fig. 5a). We identified 169 DEMs in db/db mice, with 22 upregulated and 147 downregulated (Fig. 5b, Table S11). These perinephric fat DEMs were significantly enriched in 13 pathways, involving five types of metabolic abnormalities, including energy metabolism (lipid and amino acid metabolism) and carbohydrate metabolism (Fig. 5c, Table S12). Of the 169 perinephric fat DEMs, 82 DEMs derived from microbiota and co-metabolites were screened (Fig. 5d, Table S11). Among 82 gut-derived microbial metabolites, we found that lipid and organic acid metabolites (mostly amino acid metabolites) had the greatest correlation with other metabolites (Fig. 5e, Table S13). In addition, the gut-derived microbial DEMs were mostly involved in the tryptophan, pyrimidine, and glycerophospholipid metabolism (Fig. 5f, Table S11). The expression and classification of these 82 microbe-derived metabolites are shown in Fig. 5g (Table S11), and we found that lipid and organic acid metabolites accounted for the most.

3.6. Kidney metabolite profiling in db/db mice

Untargeted metabolic analysis of kidney samples detected 897 metabolites (positive mode: 666 and negative mode: 231). OPLS-DA analysis of kidney metabolite profiles showed differences between the db/db and db/m samples ($Q2 = 0.903$, $R2 = 0.992$) (Fig. 6a). We identified 337 DEMs in db/db mice, with 178 upregulated and 159 downregulated (Fig. 6b, Table S14). KEGG enrichment analysis revealed that 337 DEMs were enriched in 23 pathways, including lipid metabolism and amino acid metabolism (Fig. 6c, Table S15). According to the source analysis results of metabolites, we screened out 33 DEMs derived from microbiota and 82 DEMs derived from co-metabolites (Fig. 6d, Table S14). In metabolite-metabolite correlations, most gut-derived microbial DEMs in the network were lipids and organic acids (mostly amino acid metabolites) (Fig. 6e, Table S16). Moreover, these gut-derived microbial metabolites were chiefly enriched in the glycerophospholipid, arachidonic acid, and tryptophan metabolism pathways (Fig. 6f, Table S15). Fig. 6g (Table S14) shows the expression levels and classification of gut-derived microbial DEMs. We found that most of these DEMs belong to the organic acids (mostly amino acids), followed by lipids.

Gut-serum-liver-perinephric fat-kidney metabolic alterations in tryptophan metabolism and glycerophospholipid metabolism:

According to the characteristics of gut-derived microbial metabolites, we found that db/db mice were mainly characterized by disturbances in lipid and amino acid metabolism, especially glycerophospholipid and tryptophan metabolism. We observed that serotonin (5-HT), 6-hydroxymelatonin, and phosphatidylcholine (PC) were high in the feces sample of db/db group. 1-acylglycerophosphocholine (lysoPC), PC, and phosphatidate (PA) were low in the serum sample of db/db group. PA, PC, lysoPC, phosphoethanolamine, glycerone-phosphate, glycerophosphoethanolamine, CDP-choline, and CDP-ethanolamine were low in liver samples of db/db group. Phosphoethanolamine, lysoPC, PC, 5-hydroxy-L-tryptophan (5-HTP), and indoleacetaldehyde (IAld) were low in perinephric fat samples of db/db group. In addition, lysoPC, acetyl-CoA, phosphatidyl-N-dimethylethanolamine, and PC were low in kidney samples of db/db group. In contrast, 5-HTP and IAld were high in kidney samples of db/db group. Gut-serum-liver-perinephric fat-kidney metabolic alterations in tryptophan metabolism and glycerophospholipid metabolism are shown in Fig. 7. The expression levels of metabolites in the pathways are shown in Figs. 2g, 3g and 4g, 5g, and 6g.

4. Discussion

Metabolomics is widely used in diabetes research, with lipids and amino acids being the most frequently studied compounds [17]. Metabolites are the intermediate or final products of biochemical reactions, respectively, which can match the disease phenotype and reflect the biological information of genetics, drugs, food, environment, gut microbes, and host [18]. In this study, we screened metabolites derived from gut microbes and investigated their varion in gut-serum-liver-perinephric fat-kidney metabolic axis in DKD mice. The results revealed that homeostasis of microbial metabolism was disrupted in DKD mice, especially the glycerophospholipid

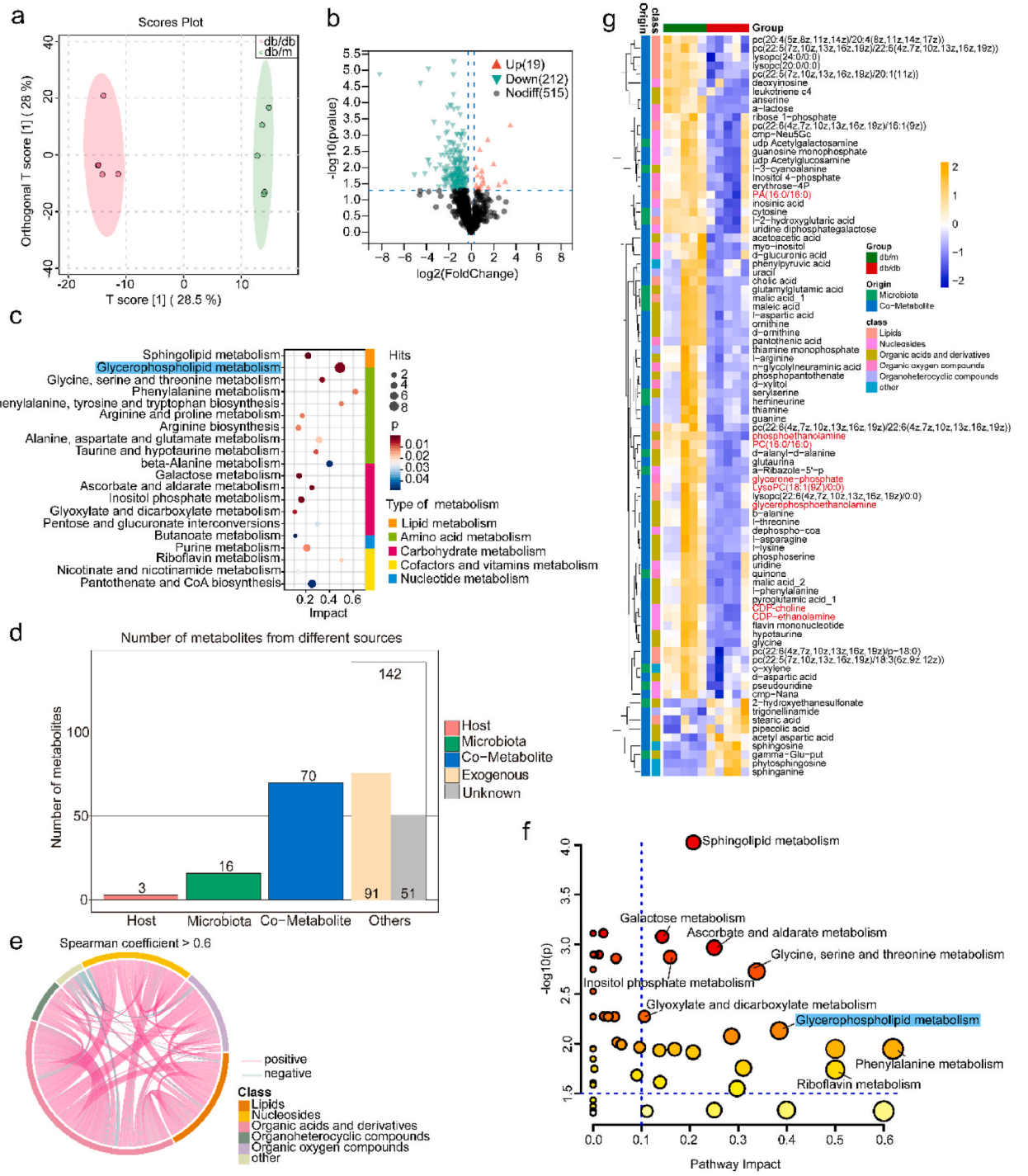

Fig. 4. Liver metabolic profiling in db/db mice. (a) OPLS-DA score showing the conspicuous differential metabolic features of liver between the db/m and db/db groups. **(b)** Volcano plot showing 231 DEMs in liver between the db/m and db/db groups. **(c)** KEGG pathway analysis of 231 liver DEMs between the db/m and db/db groups. **(d)** Column graph showing the number of liver DEMs from different sources. Co-metabolites refer to the DEMs derived from microbiota and host. **(e)** The chord diagram showing significant correlations between liver DEMs of different classes or within the same class. Metabolite class is shown as a color bar around the circumference. Each line indicates a significant correlation (Spearman's correlation, $r > 0.6$, $p < 0.05$). Pink, positive correlation; Cyan, negative correlation. **f)** KEGG pathway analysis of DEMs derived from microbiota and co-metabolites. **(g)** Heatmap of 86 DEMs derived from microbiota and co-metabolites of liver samples. Metabolite classes and origins are shown on the left of the heatmap. The red font represents DEMs in the glycerophospholipid metabolism pathway. Phosphatidate, PA; Phosphatidylcholine, PC; 1-acylglycerophosphocholine, lysoPC. (For interpretation of the references to color in this figure legend, the reader is referred to the Web version of this article.)

and tryptophan metabolism. Previous study revealed that abnormal metabolites derived from the gut microbiome can accelerate the progression of DKD [18]. Hyperglycemia disrupts the tight junctions of the gut, thereby damaging the gut barrier. Abnormal gut metabolites caused by gut dysbiosis and gut barrier disruption promote the entry of the gut microbiome and the harmful metabolites derived from them into the circulatory system, wherein they reach distant organs, such as the liver, kidneys, adipose tissue, and heart,

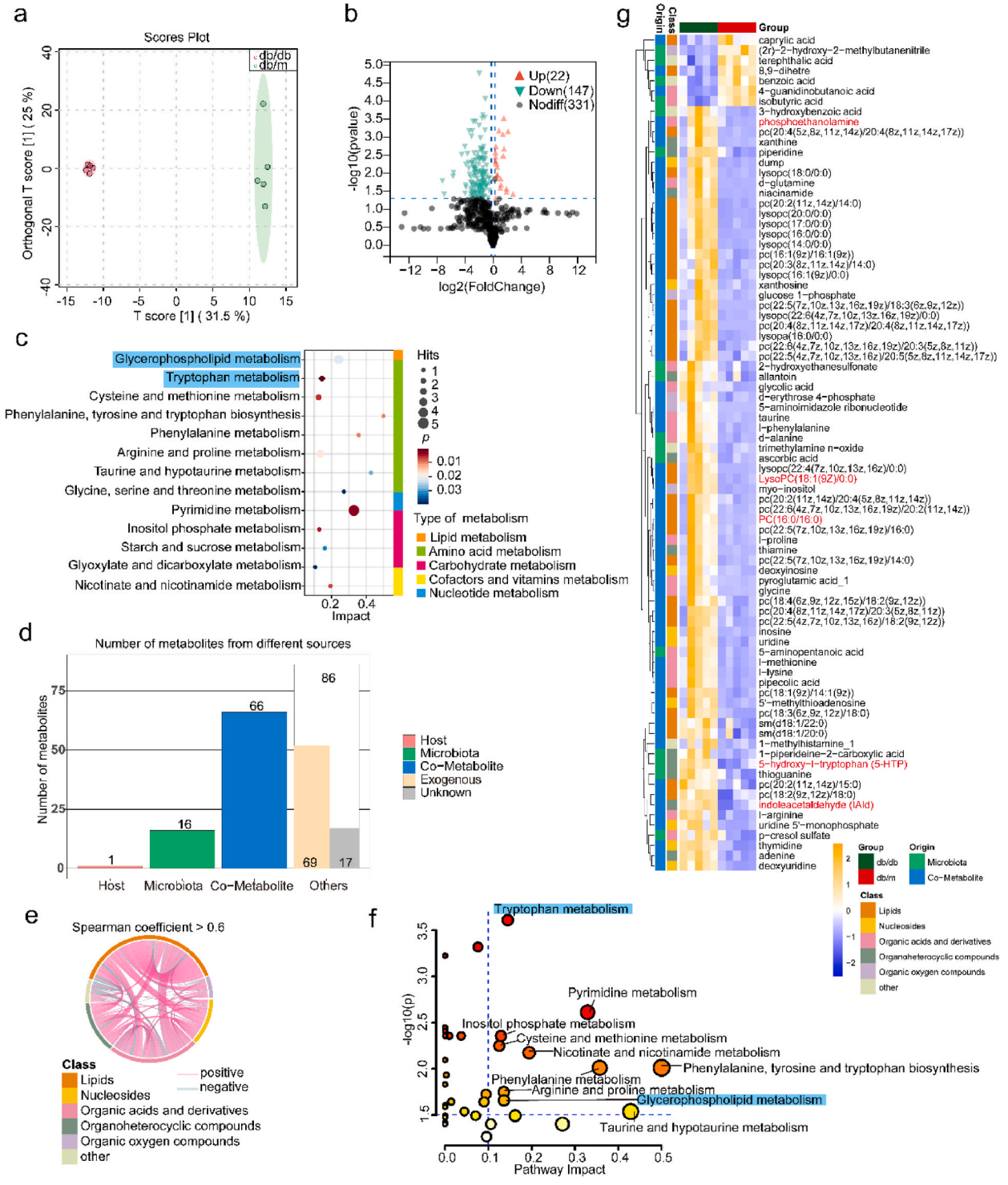

(caption on next page)

Fig. 5. Perinephric fat metabolic profiling in db/db mice. (a) OPLS-DA score showing the conspicuous differential metabolic features of perinephric fat between the db/m and db/db groups. **(b)** Volcano plot showing 169 DEMs in perinephric fat between the db/m and db/db groups. **(c)** KEGG pathway analysis of 169 perinephric fat DEMs between the db/m and db/db groups. **(d)** Column graph showing the number of perinephric fat DEMs from different sources. Co-metabolites refer to the DEMs derived from microbiota and host. **(e)** The chord diagram showing significant correlations between perinephric fat DEMs of different classes or within the same class. Metabolite class is shown as a color bar around the circumference. Each line indicates a significant correlation (Spearman's correlation, $r > 0.6$, $p < 0.05$). Pink, positive correlation; Cyan, negative correlation. **(f)** KEGG pathway analysis of DEMs derived from microbiota and co-metabolites. **(g)** Heatmap of 82 DEMs derived from microbiota and co-metabolites of perinephric fat samples. Metabolite classes and origins are shown on the left of the heatmap. The red font represents DEMs in the tryptophan metabolism and the glycerophospholipid metabolism pathways. Phosphatidate, PA; Phosphatidylcholine, PC; 1-Acylglycerophosphocholine, lysoPC. (For interpretation of the references to color in this figure legend, the reader is referred to the Web version of this article.)

and exert harmful effects.

Previous studies have demonstrated the critical effects of tryptophan metabolism on kidney diseases [22]. Zhao et al. [13] observed marked changes in tryptophan metabolism in a rat model of CKD. Tryptophan metabolism mainly constitutes three branches, including the serotonin, kynurenine, and indole derivative pathways, which are influenced by the gut microbiota. Our study found that IAld was elevated in kidney samples of db/db group. *Lactobacillus* can transform tryptophan to IAld in the presence of indole lactate dehydrogenase and aromatic amino acid aminotransferase [23]. There is compelling evidence that microbial tryptophan catabolites, such as indole, indoleacetic acid (IAA), indolelactic acid (ILA), and IAld, are essential for aryl hydrocarbon receptor (AHR) activation [24,25]. The role of AHR in renal fibrosis has been confirmed [26,27]. Activated AHR leads to glomerular and tubular cell dysfunction, resulting in interstitial fibrosis and glomerulosclerosis.

Moreover, we observed that 5-HT was high in feces of db/db mice. In line with our results, previous studies have reported high plasma 5-HT concentrations as a biomarker for assessing the early risk of DKD [28,29]. In the gut, *Ruminococcus gnavus* and *Clostridium sporogenes* breakdown tryptophan to produce tryptamine [30]. Tryptamine is converted to 5-HT in enterochromaffin cells on the intestinal mucosal surface under the key regulation of the gut microbiota [31]. Although 5-HT is not an AHR ligand, it can promote sustained AHR signaling [32]. Besides, 5-HT has been shown to enhance the production of collagen IV by human mesangial cells [33]. In addition, 5-HTP was increased in kidney samples of db/db group. Chen et al. [34] found that increased 5-HTP exacerbated tubulointerstitial fibrosis in the unilateral ureteral obstruction (UUO) rats. In all, these results indicate that the synergy of intestinal flora and tryptophan metabolism plays a crucial role in the development of DKD.

Since excess sugar can be converted into lipids, hyperglycemia can lead to a loss of balance in lipid metabolism [35]. Exploring the complex lipid metabolic pathways is beneficial for understanding the underlying mechanisms of DKD [36,37]. Small-molecule lipids, such as glycerophospholipids, including PA, PC, and phosphatidyl ethanolamines, are formed by two fatty acid (FA) molecules of the glycerol backbone. Hydrolysis of glycerophospholipids may lead to increased levels of FA, diacylglycerols, and monoacylglycerol [38], which are closely related to insulin resistance [39,40]. Under the action of phospholipase A2 (PLA2), glycerophospholipids are hydrolyzed to generate lysoPC. The accumulation of lysoPC induces insulin resistance and oxidative stress [41]. In our study, the levels of PC, PA, and lysoPC were decreased in the liver and serum samples of mice in the db/db group, while the levels of PC and lysoPC were decreased in the kidney and perinephric fat samples. In line with our results, some studies found that PC and lysoPC levels in plasma of T2D patients and animal models were lower than that in the controls [42,43]. Contrary to our results, Sun et al. [37] found that lysoPC was decreased, but PC was elevated in the kidney of the db/db group compared with the control group. However, Chen et al. [40] found decreased PC in the kidneys of T2DM rats.

Our study focused on the glycerophospholipid metabolism pathway associated with gut microbiota. We found that PC was increased in the feces sample of mice in the db/db group. PC abundant in food can be transformed into trimethylamine (TMA) under the impact of gut microbiota, such as *Anaerococcus hydrogenalis* and *Clostridium*. Then, TMA is rapidly converted to TMA-N-oxide (TMAO) under the catalysis of liver enzymes. On the one hand, TMAO promotes increased expression of bone-related molecules, resulting in calcification of smooth muscle cells and vascular tissues in CKD [44]. On the other hand, TMAO induces the expression of transcription factor FOXO1 by binding to endoplasmic reticulum stress kinase, thereby promoting hyperglycemia [45]. High levels of PC in the gut of db/db mice were broken down into TMA by gut microbes, resulting in decreased concentrations in blood, perinephric fat, liver, and kidneys. PC may act as a bridge between gut microbes and DKD progression [46]. Few studies have been conducted on glycerophospholipid metabolism pathways and gut microbes. However, further research is needed to explore the metabolic mechanisms between glycerophospholipid metabolism and gut microbiota.

4.1. Strengths & limitations

As per our knowledge, this study is the first metabolomic analysis to distinguish between host-derived, microbiota-derived, and exogenous metabolites. Using MetOrigin published in 2022 [20], we screened metabolites derived from gut microbes for analysis. In addition, given that multiple organs are involved in the progression of diabetes to diabetic nephropathy, we explored the multi-organ metabolic axis to understand the body-wide metabolic changes during disease progression. The intestinal treatment of DKD has increasingly become a research hotspot, and our results show that intestinal treatment of DKD serves as a new therapeutic strategy for DKD.

The defect of our study is the small sample size, but the modeling and operating procedures are recognized. Although we selected gut-derived metabolites, combining the gut microbiota sequencing would be better. Future studies investigating the relationship between gut microbiota and multi-organ metabolic axis would validate the findings of the current analysis.

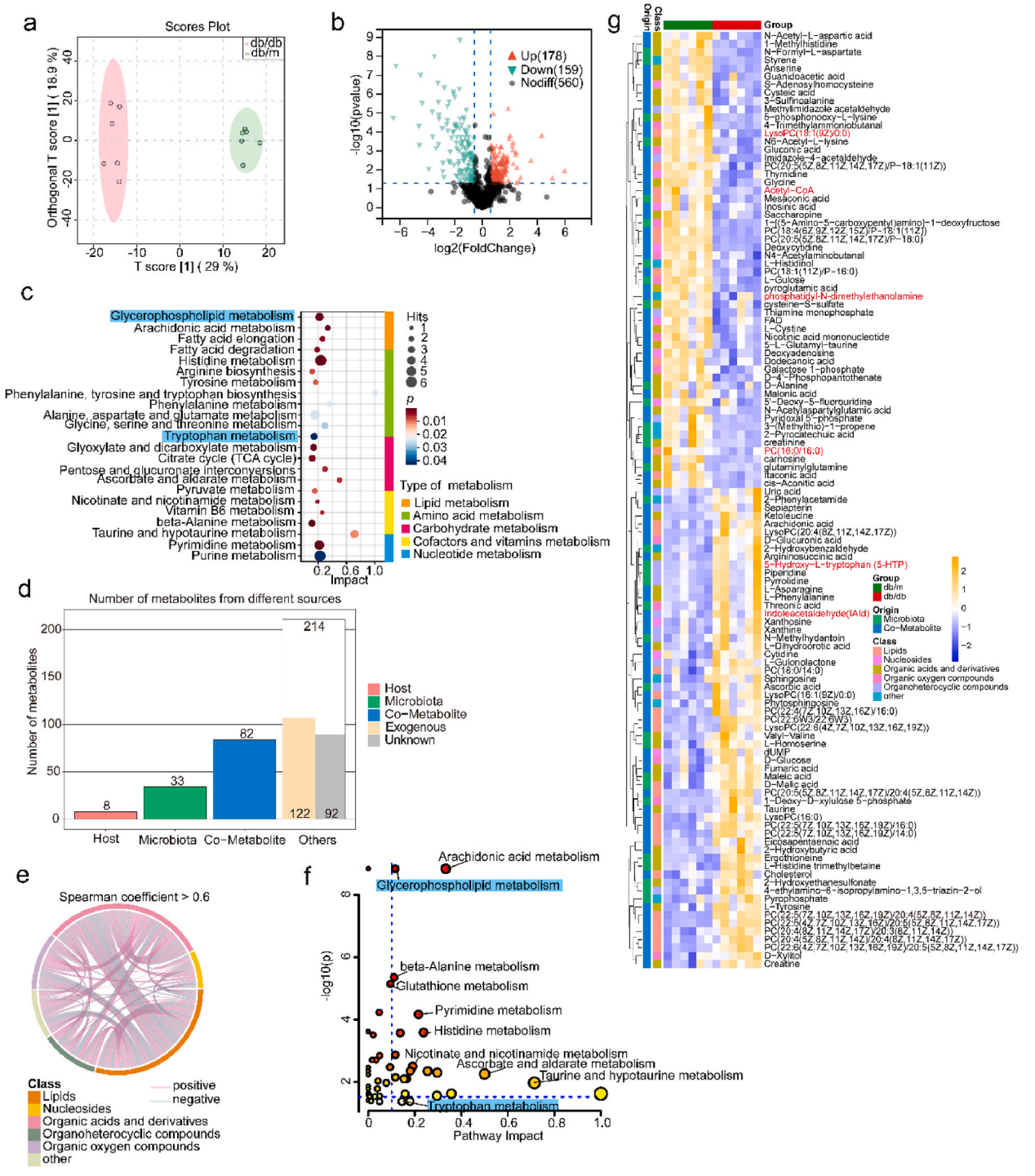

(caption on next page)

Fig. 6. Kidney metabolic profiling in db/db mice. (a) OPLS-DA score showing the conspicuous differential metabolic features of kidney between db/m and db/db group. **(b)** Volcano plot showing 337 DEMs in kidney between db/m and db/db group. **(c)** KEGG pathway analysis of 337 kidney DEMs between db/m and db/db groups. **(d)** Column graph showing the number of kidney DEMs from different sources. Co-metabolites refer to the DEMs derived from microbiota and host. **(e)** The Chord diagram showed significant correlations between kidney DEMs of different classes or within the same class. Metabolite class was shown as the color bar around the circumference. Each line indicates a significant correlation (spearman's correlation, $r > 0.6$, $p < 0.05$). Pink, positive correlation; Cyan, negative correlation. **(f)** KEGG pathway analysis of DEMs derived from microbiota and co-metabolites. **(g)** Heatmap for 115 DEMs derived from microbiota and co-metabolites in kidney samples. Metabolite classes and origins are shown on the left of the heatmap. The red font represents the DEMs in the tryptophan metabolism and the glycerophospholipid metabolism pathways. Phosphatidylcholine, PC; 1-Acylglycerophosphocholine, lysoPC. (For interpretation of the references to color in this figure legend, the reader is referred to the Web version of this article.)

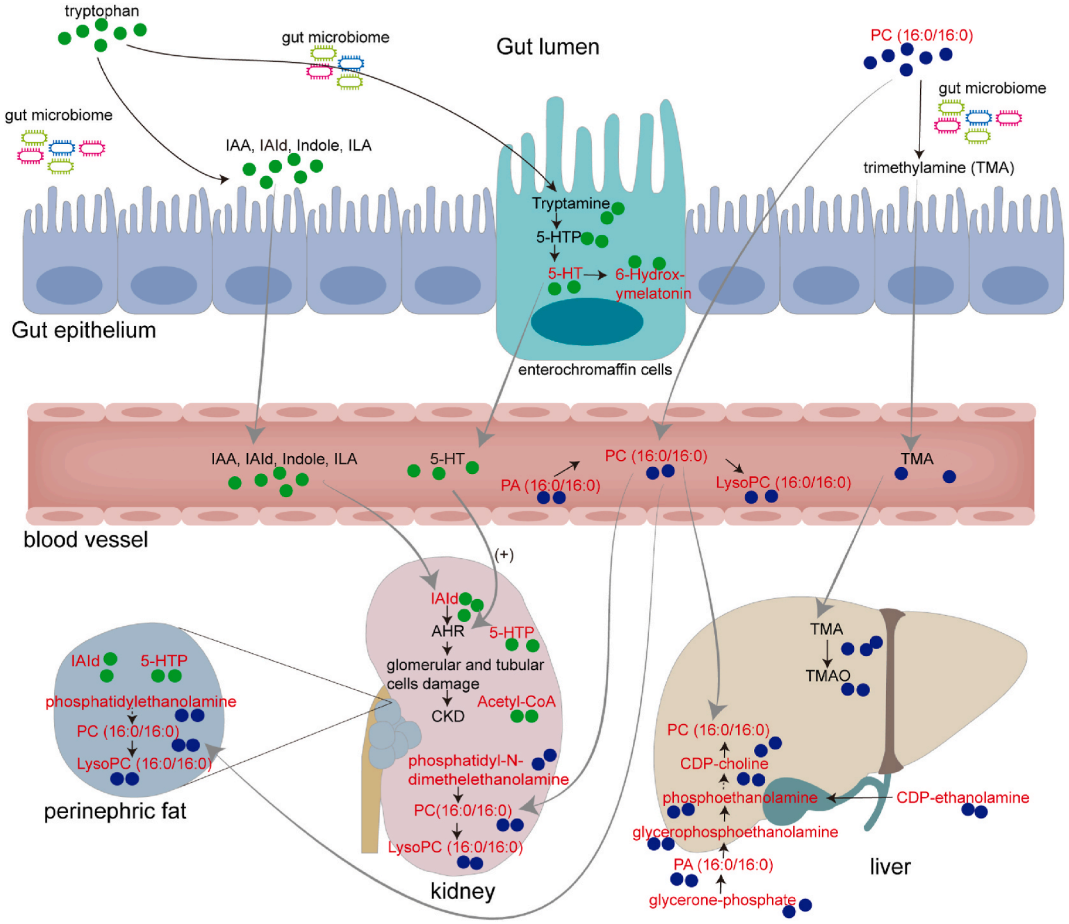

Fig. 7. Schematic diagram showing the tryptophan metabolism and glycerophospholipid metabolism under the gut microbiota control in db/db mice. The green circles represent metabolites from microbiota and co-metabolites in the tryptophan metabolism pathway. The purple circles represent metabolites from microbiota and co-metabolites in the glycerophospholipid metabolism pathway. The red font represents DEMs identified in db/db mice. Indolelactic acid, ILA; Indoleacetic acid, IAA; indoleacetaldehyde, IAld; 5-hydroxy-L-tryptophan, 5-HTP; serotonin, 5-HT; Aryl hydrocarbon receptor, AHR; Phosphatidate, PA; Phosphatidylcholine, PC; 1-Acylglycerophosphocholine, lysoPC; trimethylamine, TMA; trimethylamine N-oxide, TMAO. (For interpretation of the references to color in this figure legend, the reader is referred to the Web version of this article.)

5. Conclusion

In conclusion, we observed that microbial metabolites in gut, serum, liver, perinephric fat, and kidney of DKD mice were involved in the tryptophan and glycerophospholipid metabolism pathways. Tryptophan metabolites and glycerophospholipid metabolites were altered under the direct or indirect effects of gut microbes in peripheral organs of DKD mice. Our data revealed a global gut microbe-derived metabolic alterations across multiple organ axis in DKD mice. These findings uncover the perturbation of gut microbial metabolism in mice with DKD, which may be useful for building a bridge between the gut microbiota and the progression of DKD and provide a theoretical basis for the intestinal treatment of DKD.

Ethics approval and consent to participate

The experiments in this study were carried out in line with the requirements of the Laboratory Animal Experimentation law, and were allowed by the Experimental Animal Ethics of Jinan University (approval No. 202071-01).

Consent for publication

All the authors have read and approved the paper and declare no potential conflicts of interest in the paper. All the authors agree to publish this paper.

Author contribution statement

Ting Zhu, Bi-Ying Hu, Yi-Qing Zhang: Performed the experiments; Analyzed and interpreted the data; Contributed reagents, materials, analysis tools or data; Wrote the paper.

Ze-Yu Zhang, Kai-Wen Cai, Lei Lei, Bo Hu, Xiao-Hua Wang: Performed the experiments; Contributed reagents, materials, analysis tools or data.

Chun Tang, Yong-Ping Lu, Zhi-Hua Zheng: Conceived and designed the experiments; Analyzed and interpreted the data; Wrote the paper.

Funding statement

Dr YongPing Lu was supported by National Natural Science Foundation of China {8210032527}, Basic and Applied Basic Research Foundation of Guangdong Province {2020A1515111209}. Prof. Zhi-Hua Zheng was supported by National Natural Science Foundation of China {82170690}, The Shenzhen Science and Technology Innovation Committee of Guangdong Province of China {JCYJ20210324123200003}. Prof. Chun Tang was supported by Basic and Applied Basic Research Foundation of Guangdong Province {2019A1515110488}. Ting Zhu was supported Research start-up Fund of Postdoctoral of the Seventh Affiliated Hospital, Sun Yat-sen University {ZSQYRSFPD0030}, Postdoctoral Research Foundation of China {2021M703749}. Prof. Bo Hu was supported by Guangzhou Basic and Applied Basic Project {202201010725}.

Data availability statement

Data included in article/supp. material/referenced in article.

Declaration of competing interest

The authors have declared that no conflict of interest exists.

Acknowledgements

Not applicable.

Appendix A. Supplementary data

Supplementary data to this article can be found online at https://doi.org/10.1016/j.heliyon.2023.e17844.

Abbreviations

DM	Diabetes mellitus
DKD	diabetic kidney disease
LC-MS/MS	liquid chromatography with tandem mass spectrometry
IAld	indoleacetaldehyde
5-HTP	5-hydroxy-L-tryptophan
5-HT	serotonin
PC	phosphatidylcholine
PA	phosphatidate
lysoPC	1-acylglycerophosphocholine
CKD	chronic kidney disease
FBG	Fasting blood glucose
Cys-C	cystosin C
Ucr	Urine creatinine
ELISA	enzyme-linked immunosorbent

H&E	hematoxylin and eosin
PAS	Periodic Acid Schiff
HMDB	Human Metabolome Database
KEGG	Kyoto Encyclopedia of Genes and Genomes
TIC	total ion current
OPLS-DA	Orthogonal partial least squares discriminate analysis
VIP	Variable importance in projected
DEMs	differentially expressed metabolites
BUN	blood urea nitrogen
ILA	indolelactic acid
IAA	indoleacetic acid
AHR	Aryl hydrocarbon receptor
FA	fatty acids
PLA2	phospholipase A2
TMA	trimethylamine
TMAO	TMA-N-oxide

References

[1] S.I. Taylor, Z.S. Yazdi, A.L. Beitelshees, Pharmacological treatment of hyperglycemia in type 2 diabetes, J. Clin. Invest. 131 (2) (2021).
[2] S.M. Doshi, A.N. Friedman, Diagnosis and management of type 2 diabetic kidney disease, Clin. J. Am. Soc. Nephrol. 12 (8) (2017) 1366–1373.
[3] S. Zoungas, H. Arima, H.C. Gerstein, R.R. Holman, M. Woodward, P. Reaven, R.A. Hayward, T. Craven, R.L. Coleman, J. Chalmers, Effects of intensive glucose control on microvascular outcomes in patients with type 2 diabetes: a meta-analysis of individual participant data from randomised controlled trials, Lancet Diabetes Endocrinol. 5 (6) (2017) 431–437.
[4] H.J. Anders, T.B. Huber, B. Isermann, M. Schiffer, CKD in diabetes: diabetic kidney disease versus nondiabetic kidney disease, Nat. Rev. Nephrol. 14 (6) (2018) 361–377.
[5] C.H. Johnson, J. Ivanisevic, G. Siuzdak, Metabolomics: beyond biomarkers and towards mechanisms, Nat. Rev. Mol. Cell Biol. 17 (7) (2016) 451–459.
[6] M.M. Rinschen, J. Ivanisevic, M. Giera, G. Siuzdak, Identification of bioactive metabolites using activity metabolomics, Nat. Rev. Mol. Cell Biol. 20 (6) (2019) 353–367.
[7] Y.J. Li, X. Chen, T.K. Kwan, Y.W. Loh, J. Singer, Y. Liu, J. Ma, J. Tan, L. Macia, C.R. Mackay, S.J. Chadban, H. Wu, Dietary fiber protects against diabetic nephropathy through short-chain fatty acid-mediated activation of G protein-coupled receptors GPR43 and GPR109A, J. Am. Soc. Nephrol. 31 (6) (2020) 1267–1281.
[8] K. Kikuchi, D. Saigusa, Y. Kanemitsu, Y. Matsumoto, P. Thanai, N. Suzuki, K. Mise, H. Yamaguchi, T. Nakamura, K. Asaji, C. Mukawa, H. Tsukamoto, T. Sato, Y. Oikawa, T. Iwasaki, Y. Oe, T. Tsukimi, N.N. Fukuda, H.J. Ho, F. Nanto-Hara, J. Ogura, R. Saito, S. Nagao, Y. Ohsaki, S. Shimada, T. Suzuki, T. Toyohara, E. Mishima, H. Shima, Y. Akiyama, Y. Akiyama, M. Ichijo, T. Matsuhashi, A. Matsuo, Y. Ogata, C.C. Yang, C. Suzuki, M.C. Breeggemann, J. Heymann, M. Shimizu, S. Ogawa, N. Takahashi, T. Suzuki, Y. Owada, S. Kure, N. Mano, T. Soga, T. Wada, J.B. Kopp, S. Fukuda, A. Hozawa, M. Yamamoto, S. Ito, J. Wada, Y. Tomioka, T. Abe, Gut microbiome-derived phenyl sulfate contributes to albuminuria in diabetic kidney disease, Nat. Commun. 10 (1) (2019) 1835.
[9] V. Andrade-Oliveira, M.T. Amano, M. Correa-Costa, A. Castoldi, R.J. Felizardo, D.C. de Almeida, E.J. Bassi, P.M. Moraes-Vieira, M.I. Hiyane, A.C. Rodas, J. P. Peron, C.F. Aguiar, M.A. Reis, W.R. Ribeiro, C.J. Valduga, R. Curi, M.A. Vinolo, C.M. Ferreira, N.O. Câmara, Gut bacteria products prevent AKI induced by ischemia-reperfusion, J. Am. Soc. Nephrol. 26 (8) (2015) 1877–1888.
[10] S. Tao, L. Li, L. Li, Y. Liu, Q. Ren, M. Shi, J. Liu, J. Jiang, H. Ma, Z. Huang, Z. Xia, J. Pan, T. Wei, Y. Wang, P. Li, T. Lan, X. Tang, X. Zeng, S. Lei, H. Tang, L. Ma, P. Fu, Understanding the gut-kidney axis among biopsy-proven diabetic nephropathy, type 2 diabetes mellitus and healthy controls: an analysis of the gut microbiota composition, Acta Diabetol. 56 (5) (2019) 581–592.
[11] L. Koppe, D. Fouque, C.O. Soulage, Metabolic abnormalities in diabetes and kidney disease: role of uremic toxins, Curr. Diabetes Rep. 18 (10) (2018) 97.
[12] J.-R. Liu, H. Miao, D.-Q. Deng, N.D. Vaziri, P. Li, Y.-Y. Zhao, Gut microbiota-derived tryptophan metabolism mediates renal fibrosis by aryl hydrocarbon receptor signaling activation, Cell. Mol. Life Sci. 78 (3) (2021) 909–922.
[13] Y.L. Feng, G. Cao, D.Q. Chen, N.D. Vaziri, L. Chen, J. Zhang, M. Wang, Y. Guo, Y.Y. Zhao, Microbiome-metabolomics reveals gut microbiota associated with glycine-conjugated metabolites and polyamine metabolism in chronic kidney disease, Cell. Mol. Life Sci. 76 (24) (2019) 4961–4978.
[14] B. Zhang, Y. Wan, X. Zhou, H. Zhang, H. Zhao, L. Ma, X. Dong, M. Yan, T. Zhao, P. Li, Characteristics of serum metabolites and gut microbiota in diabetic kidney disease, Front. Pharmacol. 13 (2022), 872988.
[15] Q. Zhang, Y. Zhang, L. Zeng, G. Chen, L. Zhang, M. Liu, H. Sheng, X. Hu, J. Su, D. Zhang, F. Lu, X. Liu, L. Zhang, The role of gut microbiota and microbiota-related serum metabolites in the progression of diabetic kidney disease, Front. Pharmacol. 12 (2021), 757508.
[16] C.M. Mosterd, M. Kanbay, B.J.H. van den Born, D.H. van Raalte, E. Rampanelli, Intestinal microbiota and diabetic kidney diseases: the Role of microbiota and derived metabolites inmodulation of renal inflammation and disease progression, Best Pract. Res. Clin. Endocrinol. Metabol. 35 (3) (2021), 101484.
[17] P.R. Pereira, D.F. Carrageta, P.F. Oliveira, A. Rodrigues, M.G. Alves, M.P. Monteiro, Metabolomics as a tool for the early diagnosis and prognosis of diabetic kidney disease, Med. Res. Rev. 42 (4) (2022) 1518–1544.
[18] G. Yang, J. Wei, P. Liu, Q. Zhang, Y. Tian, G. Hou, L. Meng, Y. Xin, X. Jiang, Role of the gut microbiota in type 2 diabetes and related diseases, Metabolism 117 (2021), 154712.
[19] Y. Zhang, Z. Zhang, C. Li, D. Tang, Dai Y., Metabolomics study reveals the alteration of fatty acid oxidation in the hearts of diabetic mice by empagliflozin, Mol. Omics. 18 (7) (2022) 643–651.
[20] G. Yu, C. Xu, D. Zhang, F. Ju, Y.J.i. Ni MetOrigin, Discriminating the origins of microbial metabolites for integrative analysis of the gut microbiome and metabolome 1 (1) (2022) e10.
[21] Y.P. Lu, Z.Y. Zhang, H.W. Wu, L.J. Fang, B. Hu, C. Tang, Y.Q. Zhang, L. Yin, D.E. Tang, Z.H. Zheng, T. Zhu, Y. Dai, SGLT2 inhibitors improve kidney function and morphology by regulating renal metabolic reprogramming in mice with diabetic kidney disease, J. Transl. Med. 20 (1) (2022) 420.
[22] E. Sudar-Milovanovic, Z. Gluvic, M. Obradovic, B. Zaric, E.R. Isenovic, Tryptophan metabolism in atherosclerosis and diabetes, Curr. Med. Chem. 29 (1) (2022) 99–113.
[23] L. Cervantes-Barragan, J.N. Chai, M.D. Tianero, B. Di Luccia, P.P. Ahern, J. Merriman, V.S. Cortez, M.G. Caparon, M.S. Donia, S. Gilfillan, M. Cella, J.I. Gordon, C.S. Hsieh, M. Colonna, Lactobacillus reuteri induces gut intraepithelial CD4(+)CD8αα(+) T cells, Science 357 (6353) (2017) 806–810.
[24] M. Sun, N. Ma, T. He, L.J. Johnston, X. Ma, Tryptophan (Trp) modulates gut homeostasis via aryl hydrocarbon receptor (AhR), Crit. Rev. Food Sci. Nutr. 60 (10) (2020) 1760–1768.

[25] M. Platten, E.A.A. Nollen, U.F. Röhrig, F. Fallarino, C.A. Opitz, Tryptophan metabolism as a common therapeutic target in cancer, neurodegeneration and beyond, Nat. Rev. Drug Discov. 18 (5) (2019) 379–401.
[26] J.R. Liu, H. Miao, D.Q. Deng, N.D. Vaziri, P. Li, Y.Y. Zhao, Gut microbiota-derived tryptophan metabolism mediates renal fibrosis by aryl hydrocarbon receptor signaling activation, Cell. Mol. Life Sci. 78 (3) (2021) 909–922.
[27] S. Milanesi, S. Garibaldi, M. Saio, G. Ghigliotti, D. Picciotto, P. Ameri, G. Garibotto, C. Barisione, D. Verzola, Indoxyl sulfate induces renal fibroblast activation through a targetable heat shock protein 90-dependent pathway, Oxid. Med. Cell. Longev. 2019 (2019), 2050183.
[28] K. Hara, Y. Hirowatari, Y. Shimura, H. Takahashi, Serotonin levels in platelet-poor plasma and whole blood in people with type 2 diabetes with chronic kidney disease, Diabetes Res. Clin. Pract. 94 (2) (2011) 167–171.
[29] J. Saito, E. Suzuki, Y. Tajima, K. Takami, Y. Horikawa, J. Takeda, Increased plasma serotonin metabolite 5-hydroxyindole acetic acid concentrations are associated with impaired systolic and late diastolic forward flows during cardiac cycle and elevated resistive index at popliteal artery and renal insufficiency in type 2 diabetic patients with microalbuminuria, Endocr. J. 63 (1) (2016) 69–76.
[30] B.B. Williams, A.H. Van Benschoten, P. Cimermancic, M.S. Donia, M. Zimmermann, M. Taketani, A. Ishihara, P.C. Kashyap, J.S. Fraser, M.A. Fischbach, Discovery and characterization of gut microbiota decarboxylases that can produce the neurotransmitter tryptamine, Cell Host Microbe 16 (4) (2014) 495–503.
[31] H.M. Roager, T.R. Licht, Microbial tryptophan catabolites in health and disease, Nat. Commun. 9 (1) (2018) 3294.
[32] C.R. Manzella, M. Ackerman, M. Singhal, A.L. Ticho, J. Ceh, W.A. Alrefai, S. Saksena, P.K. Dudeja, R.K. Gill, Serotonin modulates AhR activation by interfering with CYP1A1-mediated clearance of AhR ligands, Cell. Physiol. Biochem. 54 (1) (2020) 126–141.
[33] Y. Yang, H. Huang, Z. Xu, J.-K. Duan, Serotonin and its receptor as a new antioxidant therapeutic target for diabetic kidney disease, 7680576, J. Diabetes Res. 2017 (2017) 7680576.
[34] L. Chen, D.Q. Chen, J.R. Liu, J. Zhang, N.D. Vaziri, S. Zhuang, H. Chen, Y.L. Feng, Y. Guo, Y.Y. Zhao, Unilateral ureteral obstruction causes gut microbial dysbiosis and metabolome disorders contributing to tubulointerstitial fibrosis, Exp. Mol. Med. 51 (3) (2019) 1–18.
[35] Y. Zhan, J. Wang, X. He, M. Huang, X. Yang, L. He, Y. Qiu, Y. Lou, Plasma metabolites, especially lipid metabolites, are altered in pregnant women with gestational diabetes mellitus, Clin. Chim. Acta 517 (2021) 139–148.
[36] F. Afshinnia, T.M. Rajendiran, S. Wernisch, T. Soni, A. Jadoon, A. Karnovsky, G. Michailidis, S. Pennathur, Lipidomics and biomarker discovery in kidney disease, Semin. Nephrol. 38 (2) (2018) 127–141.
[37] L. Sun, Z. Yang, W. Zhao, Q. Chen, H. Bai, S. Wang, L. Yang, C. Bi, Y. Shi, Y. Liu, Integrated lipidomics, transcriptomics and network pharmacology analysis to reveal the mechanisms of Danggui Buxue Decoction in the treatment of diabetic nephropathy in type 2 diabetes mellitus, J. Ethnopharmacol. 283 (2022), 114699.
[38] P. Castro-Gómez, A. Garcia-Serrano, F. Visioli, J. Fontecha, Relevance of dietary glycerophospholipids and sphingolipids to human health, Prostaglandins Leukot. Essent. Fatty Acids 101 (2015) 41–51.
[39] D. Lin, Y. Qi, C. Huang, M. Wu, C. Wang, F. Li, C. Yang, L. Yan, M. Ren, K. Sun, Associations of lipid parameters with insulin resistance and diabetes: a population-based study, Clin Nutr 37 (4) (2018) 1423–1429.
[40] H. Chen, Q. Nie, J. Hu, X. Huang, K. Zhang, S. Nie, Glucomannans alleviated the progression of diabetic kidney disease by improving kidney metabolic disturbance, Mol. Nutr. Food Res. 63 (12) (2019), e1801008.
[41] W. Jiang, L. Gao, P. Li, H. Kan, J. Qu, L. Men, Z. Liu, Z. Liu, Metabonomics study of the therapeutic mechanism of fenugreek galactomannan on diabetic hyperglycemia in rats, by ultra-performance liquid chromatography coupled with quadrupole time-of-flight mass spectrometry, J Chromatogr B Analyt Technol Biomed Life Sci 1044–1045 (2017) 8–16.
[42] M. Lai, Y. Liu, G.V. Ronnett, A. Wu, B.J. Cox, F.F. Dai, H.L. Röst, E.P. Gunderson, M.B. Wheeler, Amino acid and lipid metabolism in post-gestational diabetes and progression to type 2 diabetes: a metabolic profiling study, PLoS Med. 17 (5) (2020), e1003112.
[43] Z. Yan, H. Wu, H. Zhou, S. Chen, Y. He, W. Zhang, T. Chen, H. Yao, W. Su, Integrated metabolomics and gut microbiome to the effects and mechanisms of naoxintong capsule on type 2 diabetes in rats, Sci. Rep. 10 (1) (2020), 10829.
[44] X. Zhang, Y. Li, P. Yang, X. Liu, L. Lu, Y. Chen, X. Zhong, Z. Li, H. Liu, C. Ou, J. Yan, M. Chen, Trimethylamine-N-Oxide promotes vascular calcification through activation of NLRP3 (Nucleotide-Binding domain, leucine-rich-containing family, pyrin domain-containing-3) inflammasome and NF-κB (nuclear factor κB) signals, Arterioscler. Thromb. Vasc. Biol. 40 (3) (2020) 751–765.
[45] S. Chen, A. Henderson, M.C. Petriello, K.A. Romano, M. Gearing, J. Miao, M. Schell, W.J. Sandoval-Espinola, J. Tao, B.J.C.M. Sha, e5, Trimethylamine N-oxide binds and activates PERK to promote metabolic dysfunction 30 (6) (2019) 1141–1151.
[46] D. Li, J. Kirsop, W.H.W. Tang, Listening to our gut: contribution of gut microbiota and cardiovascular risk in diabetes pathogenesis, 63, Curr. Diabetes Rep. 15 (9) (2015) 63.